Molecular Vision 2022; 28:412-431 <http://www.molvis.org/molvis/v28/412>
Received 9 November 2021 | Accepted 10 December 2022 | Published 12 December 2022

Neural differentiation of human retinal pigment epithelial cells on alginate/gelatin substrate

Hoda Shamsnajafabadi,[1] Zahra-soheila Soheili,[1] Shahram Samiee,[2] Hamid Ahmadieh,[3] Ehsan Ranaei Pirmardan,[4] Massoud Haghighi[5]

[1]National Institute of Genetic Engineering and Biotechnology, Tehran, Iran; [2]Ophthalmic Research Center, Research Institute for Ophthalmology and Vision Science, Shahid Beheshti University of Medical Sciences, Tehran, Iran; [3]Blood Transfusion Research Center High Institute for Research and Education in Transfusion Medicine, Tehran, Iran; [4]Molecular Biomarkers Nano-imaging Laboratory, Brigham & Women's Hospital, Department of Radiology, Harvard Medical School, Boston, MA; [5]Gynecologist and obstetrician, Aban hospital, Tehran, Iran

Purpose: The development of biomaterials provides potent promise for the regeneration of neuroretinal cells in degenerative eye diseases and retinal tissue engineering. Biomimetic three-dimensional (3D) microenvironments and specific growth factors motivate the differentiation of human retinal pigment epithelial (hRPE) cells toward a retinal neural lineage. In this study, we evaluated alginate/gelatin (A/G) as a substrate for the culture of hRPE cells.

Methods: hRPE cells were isolated from neonatal human cadaver globes and cultivated on A/G substrate under different culture conditions, including 30% human amniotic fluid (HAF), 10% fetal bovine serum (FBS), and serum-free Dulbecco's modified Eagle's medium/nutrient mixture F-12 (DMEM/F12). The proliferation of cells in different culture conditions was determined using 3-(4,5-dimethylthiazol-2-yl)-2,5-diphenyltetrazolium bromide and a cell proliferation assay. Immunocytochemistry and real-time PCR were performed to evaluate the effect of the substrate on hRPE cell differentiation.

Results: A significant increase in the cell proliferation rate was observed in hRPE cells cultivated on an A/G substrate. Continuous observations demonstrated that hRPE cells formed densely packed, suspended spheroids in DMEM/F12 culture conditions, with dominant transdifferentiation into amacrine cells. Small adherent clusters of hRPE cells in HAF- and FBS-treated cultures represented dedifferentiation toward retinal progenitor cells. These cultures generated amacrine, rod photoreceptors, and bipolar cells.

Conclusions: These findings indicated that A/G substrate induced neural retinal cell propagation in cultures and would therefore be promising for RPE-based tissue engineering studies.

Retinal degenerative disorders, such as age-related macular degeneration (AMD) and retinitis pigmentosa (RP), are the leading causes of untreatable blindness worldwide. Several strategies are under investigation for the treatment and repair of the aforementioned disorders. Among these strategies, retinal cell transplantation is one of the most promising therapeutic approaches [1]. A wide range of cells, including embryonic stem cells, adult stem cells, induced pluripotent stem cells, retinal progenitor cells, and RPE cells, have been recruited for retinal regeneration studies [2-6]. The RPE forms a monolayer of highly specialized pigmented cells located at the interface between the photoreceptors of the neural retina and the vascular choroid. Due to the vital role of the RPE in normal retinal structure and function, RPE-based regenerative therapies have been extensively investigated in previous studies [7,8].

AMD was the first target disease for PSC-derived RPE replacement cell therapy. Ongoing phase I clinical trials confirmed the safety and some aspects of the efficacy of these potential therapeutic approaches [9].

However, there are several challenges associated with retinal cell transplantation. Growth factors and scaffolds provide promising opportunities to improve RPE-based therapies. Scaffolds can address several issues in cell transplantation strategies, such as ensuring precise cell delivery, enhanced cell survival, reduced cell death, robust cell integration, and controlled cell differentiation [10]. Human amniotic fluid (HAF) is a natural source of various growth factors, such as epidermal growth factor (EGF), fibroblast growth factor (FGF), nerve growth factor (NGF), hepatocyte growth factor (HGF), transforming growth factor alpha (TGF-a), transforming growth factor beta (TGF-b1), insulin-like

Correspondence to: Zahra-Soheila Soheili, Ministry of Science, Research and Technology, National Institute of Genetic Engineering and Biotechnology, P.O. Box: 14965/161, Pajoohesh Boulevard, 17th Kilometers, Tehran-Karaj Highway, Tehran-Iran, Postal Code: 1497716316; Phone: +98-21-44787379; FAX: +98-21-44787399; email: soheili@nigeb.ac.ir.

growth factor-I (IGF-I), insulin-like growth factor-II (IGF-II), erythropoietin (EPO), granulocyte colony stimulating factor (G-CSF), and macrophage colony stimulating factor (M-CSF). These factors represent a complex physiologic and protective liquid that surrounds the fetus. Amniotic fluid possesses broad immunosuppressive properties and has been proposed for the treatment of chronic inflammation and immune responses [11]. Our previous studies demonstrated that HAF affects the dedifferentiation and transdifferentiation of human retinal pigment epithelial (hRPE) cells to neural retinal cells [12-14].

Tissue engineering is a rapidly expanding interdisciplinary field that combines biology, medicine, and engineering. It uses a combination of cells, biologic, or synthetic materials, and specific biochemical factors to improve organ and tissue functions that have been lost due to the pathological effects of related diseases, injuries, aging, and congenital deformities. Regenerative medicine, which uses stem/progenitor cells to produce new tissues, is sometimes synonymously referred to as tissue engineering. Tissues are histologically composed of multiple types of cells and extracellular matrix proteins that comprise three-dimensional (3D) structures. In fact, traditional methods of cell growth on two-dimensional (2D) Petri dish surfaces are insufficient for cell biology assays because they do not accurately represent in vivo conditions. 2D surfaces do not provide mammalian cell-adhesive ligands, sequences in the extracellular matrix (ECM), or proteins that mimic ligands of integrin-mediating cell adhesion that facilitate cell attachment [15, 16].

To more precisely study developmental biology, scientists have designed 3D cell culture matrices. In tissue engineering therapy, scaffolds are used as 3D matrices that induce cell adhesion, proliferation, and differentiation. These scaffolds should have high biocompatibility and should not cause serious systemic or immunogenic issues during in vivo degradation and absorption. Scaffold-guided tissue engineering is used to create functional and transplantable tissue constructs. To date, a large library of synthetic and natural scaffold materials has been investigated for tissue engineering applications [17]. Alginate is composed of a family of natural linear anionic polysaccharides derived from the cell walls of marine brown algae. Gelatin is a purified protein that emerges after the thermal, chemical, or physical denaturation of collagen. Due to gelatin's valuable biologic origin, commercial availability, low cost, excellent biocompatibility, nonimmunogenicity, and appropriate biodegradability, it has been successfully employed in various biomedical applications [18].

Previous studies have shown that the negative charges of alginate reduce the proliferation and adhesion of RPE cells on purified alginate films [19]. Alginate has been applied in combination with gelatin, chitosan, elastin, agarose, or hyaluronic acid [20, 21]. This increases its biologic activity and improves its properties, ensuring cell proliferation and differentiation in vitro. Furthermore, its mechanical properties imitate native tissues [22-24]. Gelatin is a type of collagen of animal origin [25] that is biocompatible, with no induction of immune responses in the body and an absence of toxicity. Therefore, it is used in the food industry, pharmacy, wound healing, drug delivery, and gene therapy. It is frequently used in cell cultures due to its bioactive sequences, which enable a suitable microenvironment for cell adhesion, migration, proliferation, and differentiation [23, 26]. However, gelatin is soluble at 30–40 °C and passes from a gel state to a solution, limiting its application in transplantation. To prolong its degradation time and increase its water resistance, it is necessary to apply a cross-linking procedure to improve the half-life of the meshwork [27].

Cells adequately interact with the ECM in a 3D state on alginate–gelatin hydrogel scaffolds, and cocultures of multiple cell types mimic the microenvironment. The biocompatibility, biodegradability, and nontoxicity of alginate–gelatin hydrogels depend on their interactions and tissue or body fluids. The low interfacial free energy of the hydrophilic surface leads to a low tendency for proteins and cells to adhere to this surface, which makes it satisfactorily biocompatible [28,29]. Flexibility and soft structures enable this hydrated polymeric biomaterial to be used in biomedical fields as an ECM substitute in various forms, such as hydrogels, microcapsules, microspheres, fibers, foams, and sponges [30, 31]. Porosity is an important aspect, since substantial surface areas promote the attachment and growth of cells. Further, pores and channels enable the transport of gases, nutrients, and waste [22]. Alginate-hydrogel-based cell constructs are promising candidates for tissue engineering and regenerative medicine. Therefore, clinical applications are expected in the near future.

Previously, we reported an improved growth rate of hRPE cells on alginate/gelatin (A/G) scaffolds at a ratio of 20:80 [32]. The purpose of the present study was to evaluate the viability, proliferation, and death of hRPE cells cultured on an A/G film and to survey the effect of the substrate on the de- and transdifferentiation of hRPE cells under different culture conditions (30% HAF; 10% fetal bovine serum (FBS), and serum-free Dulbecco's modified Eagle's medium/nutrient mixture F-12 (DMEM/F12).

METHODS

hRPE cell isolation, cultivation, and identification: Human cadaver eyes from individuals younger than 2 years old were individually obtained from the Central Eye Bank of Iran and transferred to the National Institute of Genetic Engineering and Biotechnology (NIGEB). The Ethics Committee of the Ophthalmic Research Center approved the use of human globes for this study. The hRPE cells were isolated using enzymatic methods within the first 24 h after death. The eyes were transferred to PBS (1X; 120 mM NaCl, 20 mM KCl, 10 mM $NaPO_4$, 5 mM KPO_4, pH 7.4) in 10 cm^2 cell culture plates, and the extraocular tissues were completely removed. Each globe was cut along the ora serrata, and the anterior segment was discarded. After making four radial cuts from the edge of the eyecup, the neural retina was peeled off. The exposed RPE layer was washed with PBS, and the dark-brown pigmented RPE monolayer was completely dissected from the surrounding tissue and cut into small pieces. Then, isolated tissues were incubated in 1 U/ml dispase I solution (Roche, Mannheim, Germany) at 37 °C in a humidified atmosphere of 10% CO_2 for 50 min. The cell suspension was subsequently centrifuged at 300 × *g* for 5 min. After the supernatant was removed, isolated hRPE cells were plated in 25 cm^2 cell culture flasks (Nunc, Roskilde, Denmark). Primary cultures at 10% confluency were incubated at 37 °C in a humidified 5% CO_2 incubator until they became approximately 90% confluent (1 × 10^6 cells in T25 flask). The cultures were re-fed every 3–4 days with fresh DMEM/F12 media supplemented with 10% FBS. Subconfluent cell cultures were subcultured at a 1:3 ratio (3× 10^5 cells in T25 flask) using 0.25% trypsin-1 mM EDTA (T/E) solution.

Standard immunostaining was performed using rabbit polyclonal anti-human RPE65 antibody (Santa Cruz Biotechnology, sc-32893) to verify the identity of the isolated cells according to the manufacturer's protocol. Negative controls (secondary antibodies only) and background controls (no antibodies) were also included in the experiments (Appendix 1). Three globes (donors aged between 2 months and 2 years old) were included to provide variety in the experimental cultures.

Alginate/gelatin gel preparation: To prepare a fitting A/G substrate, a sodium alginate solution (2%; Aldrich, Munich, Germany) was prepared in distilled water at room temperature. An aqueous solution of 8% (w/v) gelatin (Sigma, Munich, Germany) in distilled water was prepared by stirring at 50 °C. A 20:80 weight ratio of A/G blend was prepared by mixing alginate and gelatin stock solutions. To prepare an A/G substrate of 1 mm thickness, 320 µl of A/G blend was transferred into each well of a polystyrene 12-well microplate and chilled at −70 °C for 20 min. The resulting A/G scaffold was crosslinked by adding 500 µl 2% (w/v) $CaCl_2$-$2H_2O$ (pH 7.2; Merck, Darmstadt, Germany) and incubating for 1 h at room temperature. Subsequently, the substrate was washed with sterilized water to remove free calcium ions and then equilibrated by the addition of 500 µl DMEM/F12 (Sigma, Munich, Germany) media, followed by incubation for 4 h in a cell culture incubator.

HAF preparation: Amniotic fluid samples were obtained from 30 pregnant women who underwent amniocentesis between the 14th and 16th weeks of pregnancy for the assessment of genetic deficiencies. Amniotic fluid cells were removed for karyotype analysis by centrifugation at 300 × *g* and 4 °C for 5 min. The resulting supernatants were sterilized using a 0.2 µm membrane filter (Orange Scientific, Brussels, Belgium) and stored at −70 °C until analysis. Cell-free supernatants, in cases with no evidence of chromosomal abnormalities, were pooled and used in downstream experimental procedures, including cell viability, cell death, cell proliferation, quantitative real-time PCR, and immunostaining assays. The procedure used to collect the samples was approved by the Ophthalmic Research Center (ORC).

hRPE cell culture on an A/G substrate: A previous study demonstrated that 30% HAF, compared to 20% HAF and 10% HAF, effectively stimulated the proliferation and differentiation of hRPE cells into retinal neurons [14]. Cultures from Passage 4 were used (1 × 10^5 cells/well) to seed cells on A/G substrate in 12-well microplates (Nunc). DMEM/F12 culture media supplemented with either 30% HAF or 10% FBS (Gibco, Karlsruhe, Germany) were added (1 ml) to nourish the cells for 7 days. Cultures were continuously examined and imaged using phase-contrast microscopy (Axiophot Zeiss, Germany), and morphological changes were reported.

Cell viability assay: Cells from Passage 4 were seeded (1 × 10^5 cells/well) on A/G substrate in 12-well microplates (Nunc), and 1 ml DMEM/F12 culture media was added and supplemented with either 30% HAF or 10% FBS. Cells cultivated on polystyrene substrates were used as controls. Cultures were incubated at 37 °C in a humidified 5% CO_2 incubator. After 2 days, 100 µl of 3-(4,5-dimethylthiazol-2-yl)-2,5-diphenyltetrazolium bromide (MTT; 5 mg/ml; Sigma) was added to each culture vessel and incubated for an additional 16 h. When violet crystals developed, 1 ml of SDS-HCl (10% SDS/1% 1 N HCl; Merck) was added, and the cultures were incubated for another 18 h. Lastly, 200 µl from the supernatant of the vessels was transferred to each well of a 96-well microplate, and absorbance was measured at 580 nm with reference to 692 nm (Titertek Multiscan ELISA reader, Labsystems Multiskan, Roden, Netherlands) [33].

Table 1. Primers that have been used for real-rime quantitative PCR.

Official symbol	Catalog number	Amplicon length (bp)
Nestin	QT00235781	75
PKCα	QT00095746	97
CRABPI	QT00197127	101
SOX2	QT00237601	64
PAX6	QT00071169	113
VSX-2	QT00221081	145
Thy-1	QT00023569	126
Rhodopsin	QT00035700	77
GAPDH	QT01192646	119

Three independent experiments were performed with at least three replicates each.

Cell death and cell proliferation assay: Cell proliferation and cell death enzyme-linked immunosorbent assays (ELISAs) were performed to evaluate the effect of the A/G substrate on the proliferation or unfavorable apoptosis of hRPE cells in culture. As mentioned previously, A/G substrates were placed in each well of a 96-well microplate. At Passage 4, cells were seeded (1×10^4 cells) on A/G substrate in the presence of 200 µL DMEM/F12 culture media without serum or supplemented with either 30% HAF or 10% FBS and incubated at 37 °C in a 5% CO_2 incubator for 2 days. Cultures on polystyrene substrates that underwent similar treatments were assessed as controls. Cell proliferation and cell death assays were performed according to the manufacturer's instructions (cell proliferation ELISA, BrdU colorimetric, and cell death detection ELISA kits, Roche, Grenzach-Wyhlen, Germany). The results are presented as the means of three independent experiments performed at least in triplicate.

Quantitative real-time polymerase chain reaction: Using QIAzol (Qiagen, Hilden, Germany) RNA extraction reagent, total RNA was isolated from hRPE cells (1×10^5 cells/well in a six-well microplate) that had been cultured on A/G substrate for 7 days in medium supplemented with 30% HAF, 10% FBS, or serum-free conditions. Subsequently, first-strand cDNA was synthesized using a cDNA synthesis kit (Qiagen) according to the manufacturer's instructions. Real-time PCR was performed using SYBR Green master mix (Roche) to quantitatively assess RNA expression levels of the *PAX6*, *SOX2*, *VSX-2* (visual system homeobox 2), cellular retinoic acid-binding protein (*CRABPI*), rhodopsin (*RHO*), protein kinase C (*PKCα*), *Thy-1,* and *Nestin* genes. As an internal control, the housekeeping gene glyceraldehyde phosphate dehydrogenase (*GAPDH*) was used to normalize the gene expression data. Specific primers were used from the QuantiTect Primer Assays – QIAGEN; Table 1).

Real-time PCR experimental conditions were as follows: an initial activation step at 95 °C for 10 min followed by 40 cycles of amplification that consisted of a denaturation step at 95 °C for 10 s, an annealing step (35 s at 60 °C), and finally, an extension step (15 s at 72 °C). Amplification efficiency was estimated by plotting a standard curve using appropriate serial dilutions of cDNA samples for the genes of interest and housekeeping genes. Relative gene expression was calculated using Bio-Rad software (Rel Quant UpDate for relative quantification) according to the $2^{-\Delta\Delta Ct}$ method based on threshold cycle (Ct) values. To evaluate the expression of genes of interest, real-time PCR was performed for three series of treated and control cDNA samples (corresponding cultures that had been developed on polystyrene) collected from distinct experiments. Each sample was assessed at least in triplicate.

Immunostaining: Cells from Passage 5 were cultured at 1×10^5 hRPE cells/well on the A/G substrate and treated with 30% HAF, 10% FBS, or serum-free media. After 7 days, the cultures were harvested and reattached to glass coverslips using cell spin cytocentrifugation for 5 min at 160 × *g*. Standard immunostaining protocols were performed according to the manufacturer's instructions (Santa Cruz Biotechnology). Each coverslip was individually transferred to a well in a 6-well microplate, washed three times with PBS, and fixed in ice-cold methanol (−20 °C; Merck) for 5 min at room temperature (RT). Air-dried coverslips were blocked using 1% BSA (BSA, Merck) in 1% PBST (Triton X-100, Sigma, in PBS) for 1 h at RT and incubated overnight at 4 °C with specific primary antibodies at a dilution of 1:50 in 1.5% (w/v) BSA in 1% PBST (v/v). Goat polyclonal anti-human SOX2 (Santa Cruz Biotechnology, sc-17320), rabbit polyclonal anti-human Nestin (Santa Cruz Biotechnology, sc-20978), goat polyclonal

anti-human CRABPI (Santa Cruz Biotechnology, sc-10061), rabbit polyclonal anti–human PKCα (Santa Cruz Biotechnology, sc-10800), mouse polyclonal anti-human rhodopsin (Santa Cruz Biotechnology, sc-53991), mouse polyclonal anti-human Thy-1 (Santa Cruz Biotechnology, sc-59396), goat polyclonal anti-human PAX6 (Santa Cruz Biotechnology, sc-53108), and goat polyclonal anti-human VSX2 (Santa Cruz Biotechnology, sc-21690) antibodies were applied on different coverslips. The coverslips were then thoroughly washed with PBS to reduce nonspecific antibody binding. Slides were incubated with FITC–conjugated goat anti-rabbit immunoglobulin (Santa Cruz Biotechnology, sc-2012), goat anti–mouse immunoglobulin (Santa Cruz Biotechnology, sc-2010), or donkey anti-goat immunoglobulin (Santa Cruz Biotechnology, sc-3853) at a dilution of 1:100 in 1.5% BSA in 1% PBST for 45 min at RT in the dark. Cell nuclei were counterstained with 4′,6-diamidino-2-phenylindole dihydrochloride (DAPI; Santa Cruz Biotechnology) for 10 min, and coverslips were mounted on slides using a fluorescence mounting medium (glycerol 90%, PBS 10%, and phenyl diamine 10% [w/v]). Slides were imaged using an Axiophot Zeiss fluorescence microscope equipped with a 460-nm filter and a 520-nm filter for DAPI- and FITC-labeled antibodies, respectively. Negative controls (secondary antibodies only) and background controls (no antibodies) were also included in all experiments (Appendix 2). Immunostaining tests were performed in three independent experiments.

Statistical analysis: A two-tailed Student *t* test (Microsoft Excel 2010) was used to evaluate the statistical significance of the data, and p values less than 0.05 were considered statistically significant.

RESULTS

Morphology of hRPE cells during culture: As they reached confluence, individual hRPE cells exhibited a variety of morphologies in the culture. Throughout the first 24 h to 48 h in the primary culture, the cells adhered to the flask surface and exhibited a star-like morphology with highly pigmented cytoplasm (Figure 1A).

After 3 to 4 days, cell numbers gradually increased, and a monolayer of elongated fusiform cells formed (Figure 1B). At full confluence, the cells became hexagonal and formed small, tightly packed cobblestone structures with distinct phase-bright borders (Figure 1C). During consecutive passages, the cells gradually lost their melanin granules. By Passage 5, cultures had a high proliferation rate, but eventually, cell proliferation and growth rates reduced, at which time cellular morphology changed from an elongated fusiform shape to a flattened amorphous appearance shape (data not shown). Newly developed cultures were examined by immunostaining for RPE65, which confirmed greater than 90% purity for the isolated cells and demonstrated that the cultures were RPE driven (Figure 1D).

Morphometric analysis of hRPE cells cultured on polystyrene under different culture conditions: The hRPE cells exhibited the same morphology under treatment with FBS and DMEM/F12 on polystyrene. They displayed a flattened, spindle-shaped phenotype in the control uncoated wells during the inspection of the cultures (Figure 2).

HAF treatment induced hRPE cells to form spheroids when they were cultured on polystyrene. After 24 h and 48 h, the hRPE cells displayed a flattened, spindle-shaped phenotype on polystyrene (Figure 2). After 3 days, the cells began to aggregate and formed sphere-like structures that tended to detach from the surface of the plate and float into the medium. The spheroids maintained their morphology over the next 4 days (Figure 2 and Table 2).

Morphometric analysis of hRPE cells cultured on A/G substrate under different culture conditions: The hRPE spheroids in FBS- and HAF-treated cultures were entrapped within the A/G substrate. Individual cells and small nodular spheroids were observed on A/G substrates. The cells did not attach to the substrate on the first day. Rather, they adhered to the A/G substrate 2 to 7 days after cultivation (Figure 3). Inspection of the cultures over consecutive days revealed that single cells and spheroids grew larger, their numbers increased, and dense spheroids became entrapped within the A/G substrate.

Suspended dense spheroids developed on A/G substrates in DMEM/F12-treated cultures (Figure 3). When the cultures were maintained in DMEM/F12, single cells and small nodular spheroids were detected on the A/G substrate during the first 24 h. The spheroid structures did not engage with the A/G substrate during the 7 days of consecutive inspections. The high rate of cell proliferation led to the formation of sizable cellular clumps in the cultures, which tended to aggregate and form densely packed, rounded spheroids (Table 2).

hRPE cells exhibited the same viability on A/G and polystyrene substrates: According to the colorimetric MTT assay, no significant difference was observed in the viability of hRPE cells between media supplemented with FBS ($p = 0.11$), or DMEM/F12 ($p = 0.8$), regardless of the substrate type. Cellular viability was increased in the HAF-treated cultures compared to the control ($p = 0.04$; Figure 4A-B).

A/G substrate induced proliferation in hRPE cells: According to the cell proliferation ELISA, proliferation rates increased

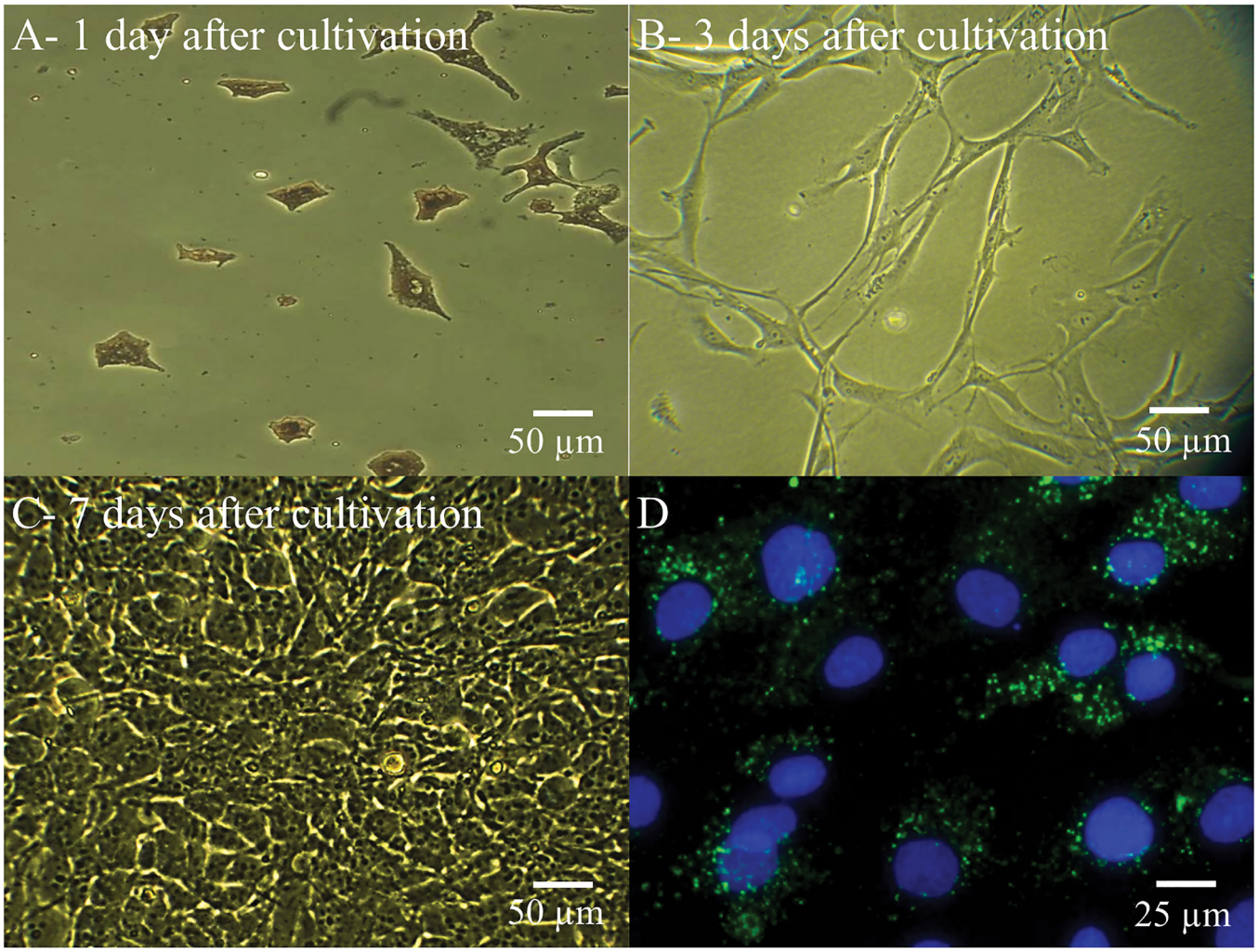

Figure 1. Phase-contrast micrograph of hRPE cells' primary culture morphologies, immunostaining for verification of the cells' identity. **A**: Polygonal cells with densely pigmented morphology of hRPE cells 1 day after cultivation. **B**: 3 days later, hRPE cells formed a monolayer of elongated fusiform cells. **C**: They made small, tightly packed cobblestone structures with distinct phase-bright borders in confluent cultures 7 days after cultivation. **D**: Merged image for the RPE65 marker (green) and DAPI nuclear staining (blue). Immunocytochemistry analysis in the 5th passage, represented that, more that 90% of hRPE cells in the population were positive for RPE65. Magnification: (A, B, and C: 320X and D: 400X).

by approximately twofold when cells were cultivated on A/G substrates, irrespective of the type of nutrient media used (HAF, p = 0.0009; FBS, p = 0.002; DMEM/F12, p = 0.008). The highest rate of hRPE cell proliferation was observed in the HAF-treated cultures, presumably due to their considerable growth factor content (Figure 4C).

The cell death ELISA demonstrated that the A/G substrate did not have a significant impact on the apoptotic rate of the hRPE cell culture when compared to the polystyrene substrate (FBS, p = 0.61; HAF, p = 0.10; DMEM/F12, p = 0.55). Cell death was significantly lower than that of the positive control included in the kit (Figure 4D).

Gene and protein expression analysis of specific retinal cell markers: According to RT–PCR data and immunostaining, the A/G substrate increased the expression levels of neural retinal progenitor (PAX6), neural stem (SOX2), late retinal progenitor (VSX2), neural progenitor cell (Nestin), amacrine (CRABPI), rod photoreceptor (RHO), bipolar (PKCα), and retinal ganglion (Thy-1) cell markers compared to the polystyrene substrate.

A/G substrate promoted the expression of stem cells or progenitor cells in hRPE cell cultures: Compared to corresponding cultures on polystyrene, the A/G substrate, did not induce *SOX2* gene expression in DMEM/F12-treated cultures, whereas considerable amounts of *SOX2* gene expression were

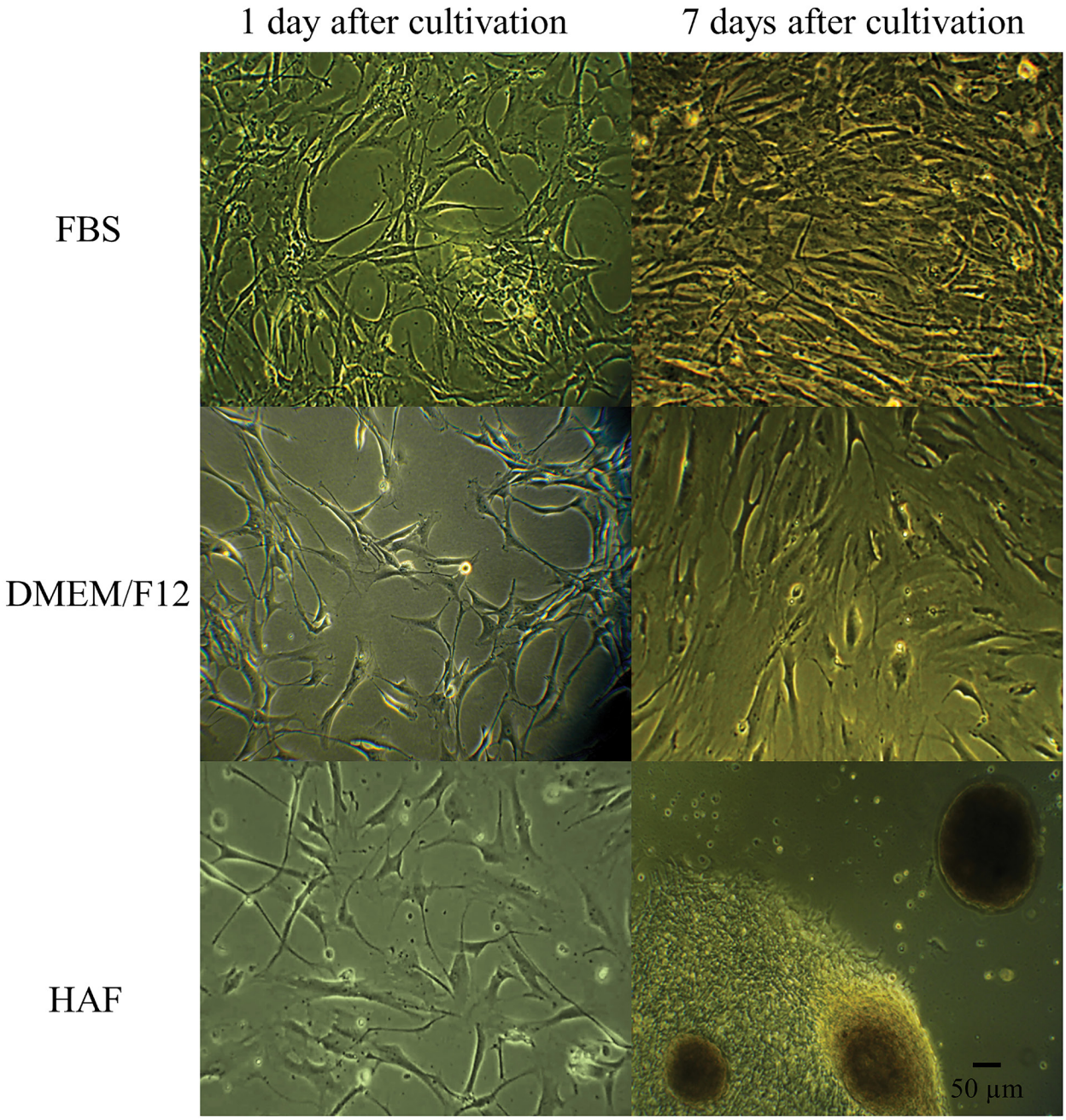

Figure 2. Phase-contrast micrograph of hRPE cell morphology on polystyrene (Passage 4) under the treatment of FBS, DMEM/F12 and HAF. Elongated fusiform morphology of the cells developed in FBS- and DMEM-treated cultures. The aforesaid structures formed in HAF-treated cultures on the first day of starting the cultures, whereas the floated and attached spheroids appeared on the 7th day of the cultures. Magnification: 200X.

detected in HAF-treated cultures (382-fold, p = 0.00002) and FBS- (43-fold, p = 0.0001) (Figure 5). SOX2 protein expression was detected in HAF-, FBS-, and DMEM/F12-treated cultures (Figure 6). Although SOX2 protein expression is generally restricted to the nucleus, cytoplasmic staining was detected in this study.

An approximately twofold increase in *Nestin* gene expression was observed in HAF- or DMEM/F12-treated cultures on A/G compared to polystyrene. A 1.3-fold

Table 2. Morphological features under different treatments.

Treatment	Cell aggregate volume	Structure	Adherence
Polystyrene + FBS	-	Single cells	-
Polystyrene + HAF	Big-Small	Spheroids and single cells	Attached and Suspended
Polystyrene + DMEM/F12	-	Single cells	-
A/G substrates + FBS	Small	Spheroids	Attached
A/G substrates + HAF	Small	Spheroids	Attached
A/G substrates + DMEM/F12	Big	Spheroids	Suspended

increase was detected in FBS-treated cultures (Figure 5). Immunostaining of hRPE cells cultured in HAF-, FBS-, or DMEM/F12-containing media showed that the positive cells expressed neural progenitor cell markers (Figure 6).

Assessment of A/G cultures with respect to cultures on polystyrene revealed that *PAX6* gene expression levels in HAF-, FBS-, and DMEM/F12-treated cultures were enhanced 695-, 177-, and 12-fold, respectively. Relative expression of *PAX6* in FBS-treated cultures was significantly higher compared to DMEM/F12- ($p = 0.0002$) and HAF- ($p = 0.00015$)-treated cells (Figure 5). Immunostaining of hRPE cells cultured in media containing HAF, FBS, and DMEM/F12 showed that the cultures were positive for PAX6, a neural retinal progenitor cell marker (Figure 7).

Lastly, *VSX-2* gene expression in HAF-, FBS-, and DMEM/F12-treated cultures was enhanced 303-, 259-, and 16-fold in A/G cultures compared to controls plated on polystyrene. The expression levels of the *VSX-2* gene in hRPE cells treated with FBS ($p = 0.00029$) and HAF ($p = 0.00024$) were much higher than those in cells treated with DMEM/F12 (Figure 5). Immunostaining results for VSX-2 revealed that hRPE cells expressed late retinal progenitor cell markers in HAF-, FBS-, and DMEM/F12-containing media (Figure 7).

A/G substrate promoted the expression of neural retinal cell markers in hRPE cell cultures: The hRPE cells in A/G demonstrated a fourfold increase in *Thy-1* gene expression under FBS treatment compared to cells grown on polystyrene (Figure 5). Immunostaining results revealed the presence of Thy-1 ganglion cell markers in DMEM/F12-treated cultures (Figure 8).

The expression levels of *PKCα* were increased fourfold in HAF-treated cultures on A/G compared to the polystyrene substrate (Figure 5). Immunostaining results for PKCα protein showed that the cells expressed bipolar cell markers in all three culture conditions (Figure 8).

The same levels of *RHO* gene expression were observed in HAF- and FBS-treated cultures, which were approximately 50-fold higher than for DMEM/F12 treatment (Figure 5). Immunostaining for rhodopsin demonstrated its expression in all culture conditions (Figure 9).

In A/G cultures, compared to polystyrene, *CRABPI* gene expression under FBS-, HAF-, and DMEM/F12-treatments

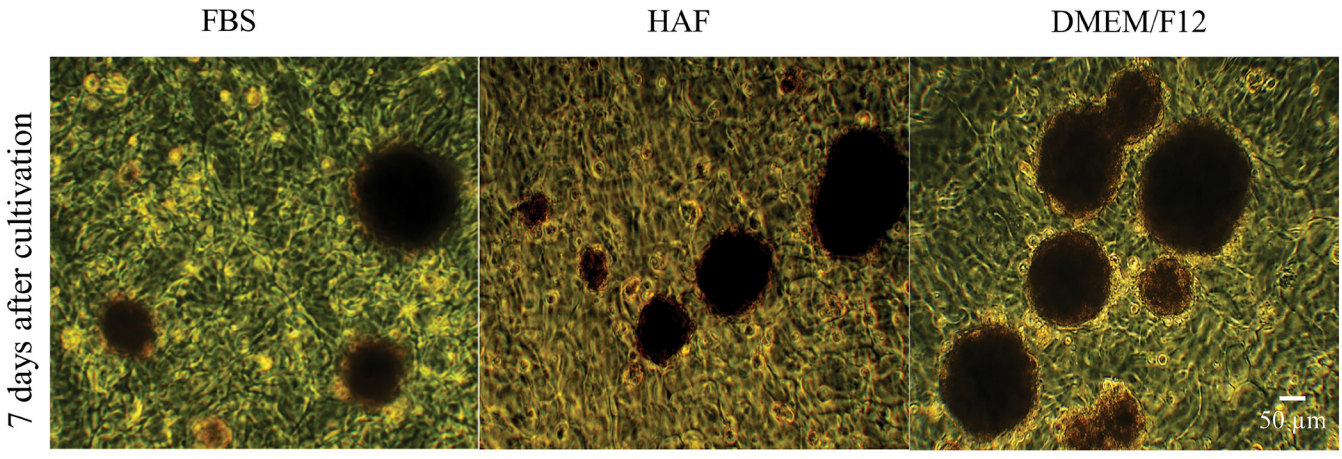

Figure 3. Phase-contrast micrograph of hRPE cells (Passage 4), on A/G substrate. The dense spheroids developed on A/G substrate in FBS, HAF and DMEM/F12 -treated cultures 7 days after cultivation. Magnification: 200X.

was enhanced 177-, 18-, and 76-fold, respectively (Figure 5). A large number of cells were positively labeled with the CRABPI antibody in the examined culture conditions (Figure 9). Schematic presentations of hRPE cell gene expression are presented in Figure 10 [34].

Since the cells mostly formed spheroids on the A/G substrate and in DMEM free of serum, accurately counting positive cells expressing individual markers was not possible. Therefore, positive cells for the investigated markers are represented qualitatively, not quantitatively.

DISCUSSION

Herein, we evaluated the competence of the A/G substrate for hRPE cell cultures under treatment with HAF- or FBS-containing media or in DMEM/F12 growth factor-free media. We tested the hypothesis that the proposed culture conditions would enhance retinal proliferation and differentiation with

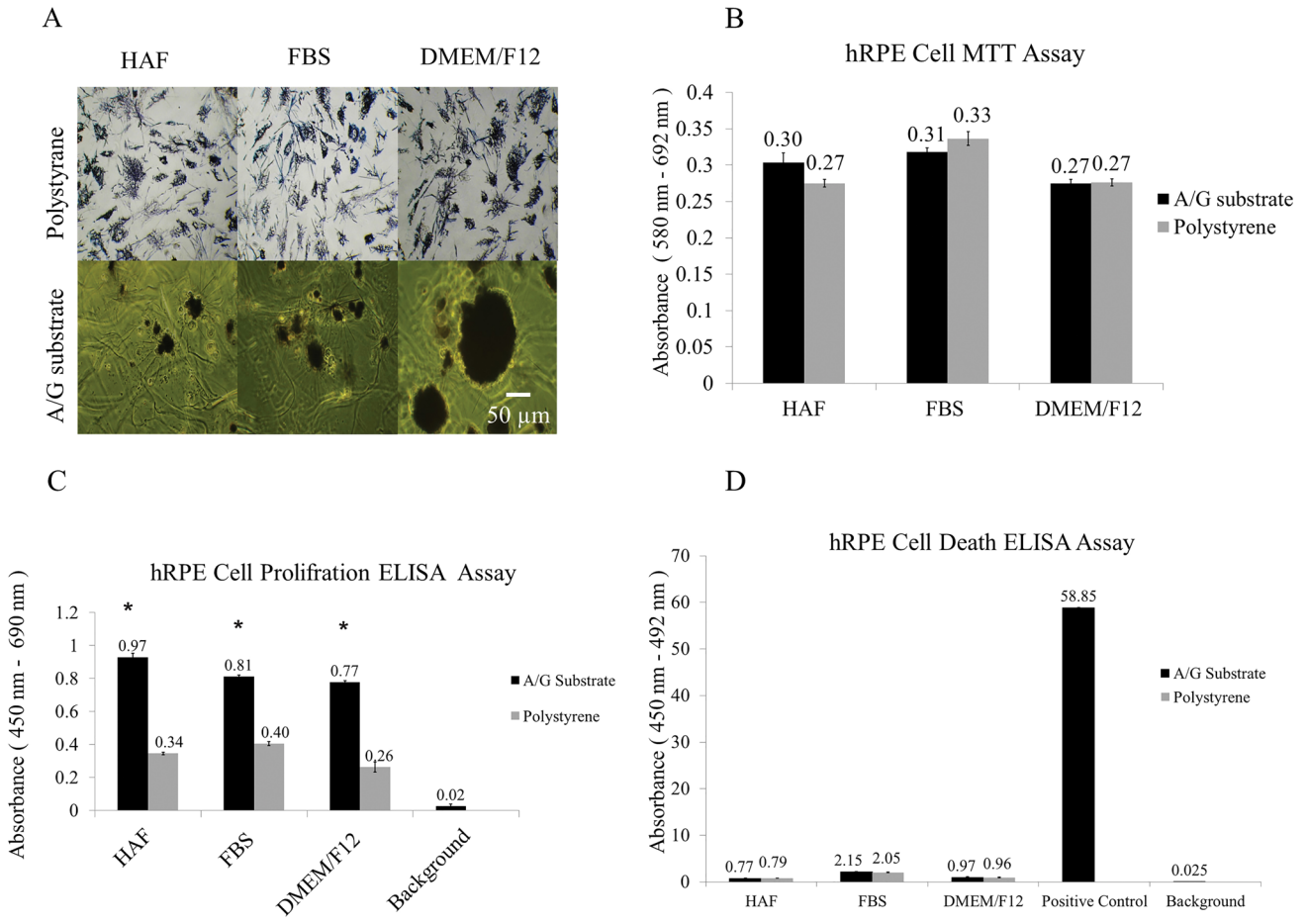

Figure 4. Phase-contrast micrograph of formazan crystals that were developed in cells (Passage 4), which had been cultured on A/G substrate and polystyrene, the bar graph of 3-(4,5-dimethylthiazol-2-yl)-2,5-diphenyltetrazolium bromide (MTT) assay, and the effect of A/G substrate on cell proliferation and apoptosis. Mitochondrial dehydrogenase enzyme in living cells reduces MTT to soluble purple formazan crystals. The absorbance of the samples was quantified by spectrophotometer. **A**: Representative formazan crystals in amniotic fluid (AF), fetal bovine serum (FBS), and Dulbecco's modified Eagle's medium/nutrient mixture F-12 (DMEM/F12)-treated hRPE cells on polystyrene and A/G substrate. **B**: The results of the MTT cell viability assay. The viability of hRPE cells on A/G substrate and polystyrene were nearly the same in HAF ($p = 0.04$), FBS ($p = 0.11$), and DMEM/F12 ($p = 0.8$). **C** and **D:** The effect of A/G substrate on cell proliferation and apoptosis, respectively. The 4th passage hRPE cells (104 cells/well) were seeded in 96-well plates, on A/G substrate and uncoated polystyrene, in 3 different aforesaid conditions. 48 h later, cell proliferation and cell death were assessed using ELISA kits. Cell proliferation was increased on A/G substrate when compared to polystyrene in HAF ($p = 0.0009$), FBS ($p = 0.002$), and DMEM/F12 ($p = 0.008$) treatments. (*$p<0.05$) Each bar represents means ± standard error of the mean (SEM) of at least three independent experiments performed in triplicate. Magnification: 200X.

respect to traditional cultures on polystyrene. The hRPE cells were routinely cultivated in DMEM/F12 supplemented with 10% FBS and displayed a flattened, spindle-shaped phenotype on polystyrene during early passages (Figure 1B). Liao and Stanzels showed that RPE cells displayed hexagonal morphology in fully confluent cultures [35, 36]. We also observed this characteristic morphology in fully confluent cultures (Figure 1C). The hRPE cells exhibited the same morphology in FBS-containing or FBS-free DMEM/F12 media when cultured on polystyrene (Figure 2). The cells exhibited normal morphology during the first 48 h in the HAF-treated culture (Figure 2). However, by day 3 in culture, they joined together and formed sphere-like structures. The spheroids detached from the surface of the plate, floated into the medium, and maintained their spheroid morphology throughout subsequent days (Figure 2). Similar to the HAF culture conditions, hRPE cells exhibited a 3D spheroid morphology on the A/G substrate (Figure 3). Several reports have indicated that spheroid formation is a desirable characteristic for applications in biomedical fields. Chen et al. demonstrated that human osteoblast cells that formed 3D clusters on Ca-alginate scaffolds provided an invaluable environment for bone-like tissue formation [37]. A study also showed that a 3D culture efficiently promoted osteogenic differentiation of mesenchymal stem cells (MSCs) [38]. It seems that spheroid formation by hRPE cells on A/G substrates establishes a potential carrier for retinal cell transplantation and retinal-like tissue formation. Spheroid formation is the first phase of cell reorganization during the fabrication of an engineered organ [39].

Studies have reported two types of cell spheroid cultures due to spontaneous interactions between cells (cell–cell) and substrates (cell–ECM). In addition to the role of growth factors in guiding cellular differentiation, signals derived from cell–cell or cell–ECM interactions also play an important role in neural cell differentiation. These messages can be mechanical, physical and/or chemical stimuli, which are received through contact with surrounding cells or the ECM, and drive differentiating cells toward particular cell lineages [40].

A/G substrate promoted cell–ECM interactions under HAF or FBS treatments. However, DMEM/F12 led to hRPE cells' interactions and finally cellular aggregates formed large suspended spheroids in cultures. In a DMEM/F12-treated culture, the A/G substrate stimulated hRPE cells to aggregate into large suspended spheroids that established cell–cell interactions (Figure 3).

MSCs exhibited adhered spheroids on alginate hydrogel similar to HAF- and FBS-treated hRPE cultures [41]. However, a human breast cancer cell line (MCF-7) formed suspended nonadherent spheroids on silicon substrate [42], similar to DMEM/F12-treated hRPE cell cultures. Under such conditions, the cells did not exhibit anchorage-dependent growth, and the size of the multicellular spheroids was dependent on the number of seeded cells [42,43].

The MTT assay results demonstrated that the A/G substrate promoted hRPE cell survival. The cells exhibited 98% viability at the end of the culture period in all experimental conditions (Figure 4A–B). Cell proliferation ELISA results revealed an increased rate of proliferation on the A/G substrate compared to polystyrene in all three culture conditions (twofold increase; Figure 4C). Spheroid formation on the A/G substrate promoted hRPE proliferation by inducing cell–cell or cell–ECM interactions. Previous studies have confirmed that the alginate substrate supports the growth of RPE cell lines, bone marrow cells, NB2a neuroblastoma cells, and H9C2 cardiomyoblasts [44-47].

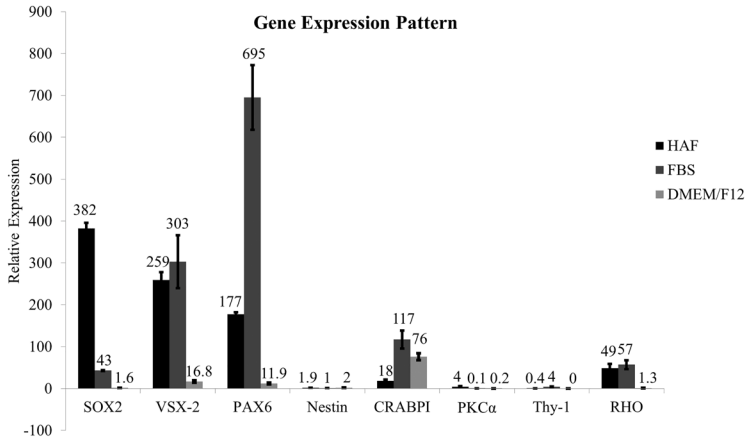

Figure 5. Relative gene expression of retinal cell markers. The bar graphs represent relative expression of neural retinal cell markers (CRABPI, RHO, PKCα and Thy-1) and neural progenitor/stem cell markers (PAX6, SOX2, VSX2, and Nestin) in HAF, FBS, and DMEM/F12–treated cultures on A/G substrate compared to polystyrene. Each bar represents the mean ± SEM of at least 3 independent experiments in at least triplicate.

Cell death ELISA demonstrated that A/G substrates did not induce significant cell death in hRPE cell cultures (Figure 4D), indicating that the A/G substrate allows the cells to absorb sufficient amounts of oxygen and nutrients. Previous studies have shown that encapsulated hRPE cells in alginate hydrogels do not display significant levels of apoptosis [48].

The highest proliferation rate was observed in HAF-treated cultures, which may be due to HAF being composed of several growth factors, e.g., transforming growth factor beta (TGF-β), complement C3, and plasminogen, which play important roles in inducing cell proliferation. The role of HAF in inducing cell proliferation in cultured hRPE cells, hematopoietic stem cells, lens cells, and human skin fibroblast cells has been previously demonstrated [12,49-51].

As cells differentiate, the proliferation rate usually decreases, and cells arrest in G_0 phase of the cell cycle [52].

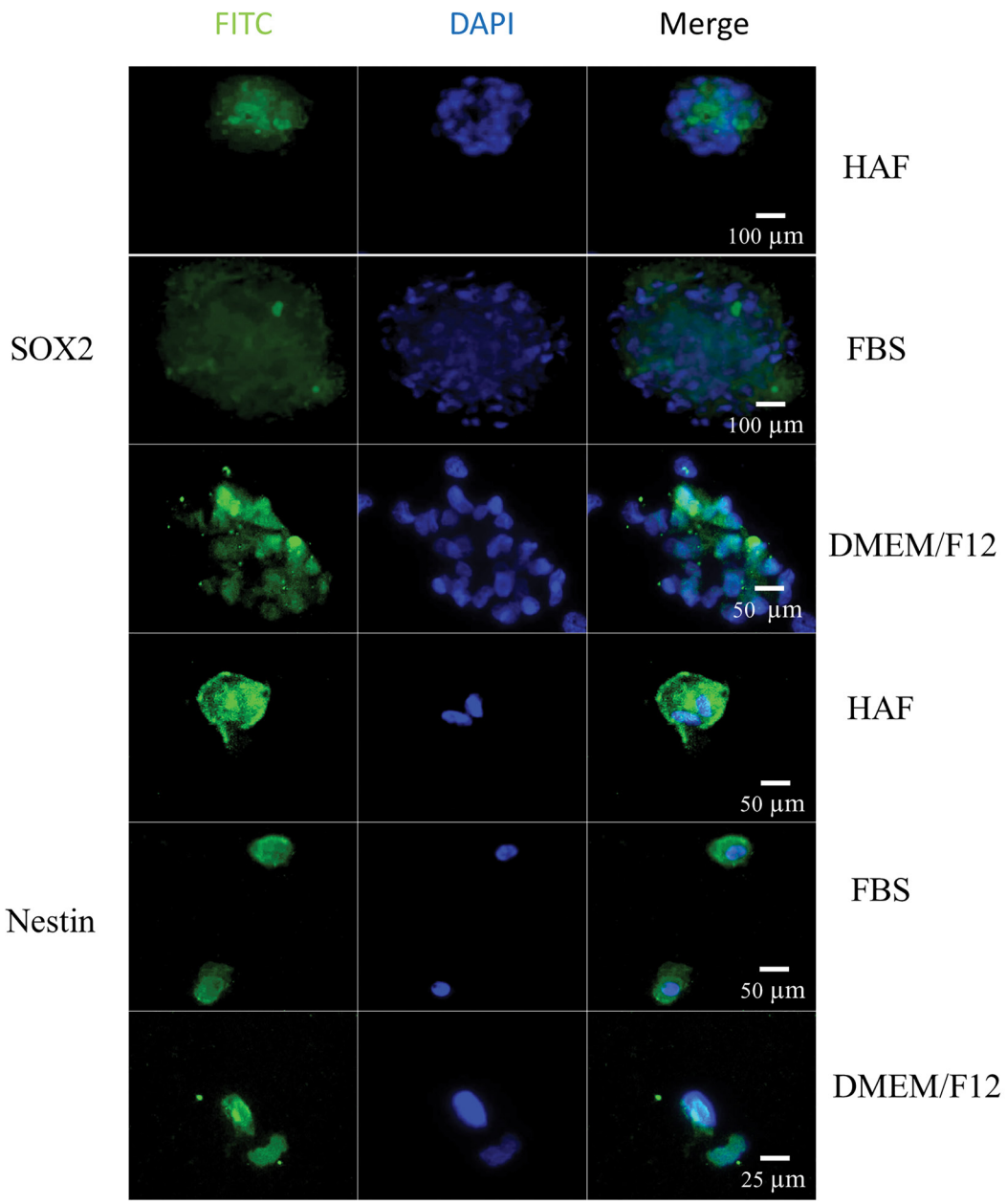

Figure 6. Immunostaining for SOX2 and Nestin markers. SOX2 nuclear and cytoplasmic expression and Nestin nuclear expression in HAF, FBS, and DMEM/F12-treated hRPE cells (passage 5) that had been cultured on A/G substrate, after 7 days. Magnification: 200X.

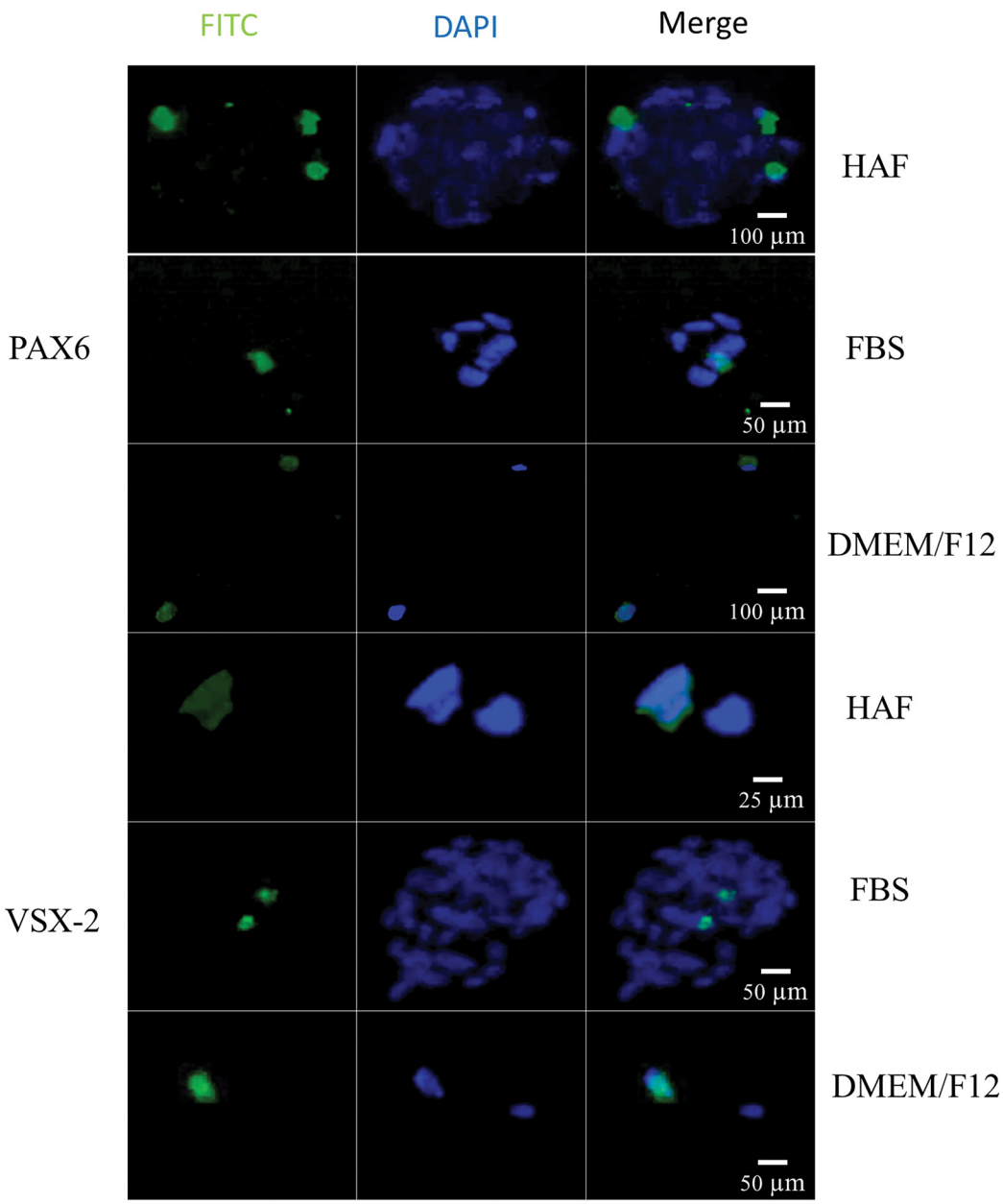

Figure 7. Immunostaining for PAX6 and VSX2 markers. PAX6 nuclear expression and VSX2 cytoplasmic expression in HAF, FBS, and DMEM/F12-treated hRPE cells (Passage 5) that had been cultured on A/G substrate, after 7 days. Magnification: 200X.

Undifferentiated retinal progenitor cell (RPC) cultures are typically characterized by their ability to proliferate in vitro [53, 54]. Our data revealed that HAF-treated cultures harbored RPCs with a high proliferation rate, while FBS- and DMEM/F12-treated cultures included neural differentiated cells with a low proliferation rate.

Real-time PCR and immunostaining data confirmed that *SOX2* was expressed under all examined conditions (Figures 5–6). Dominant *SOX2* expression was detected in the HAF-treated cultures (Figure 5). Substrate-induced cell–ECM interactions and growth factors increased the expression of neural stem cell markers. Similarly, Gao et al. reported the differentiation of multipotent human adipose-derived stromal/stem cells into neural stem cells on chitosan and gelatin 3D scaffolds [55]. SOX2 is usually expressed in the nuclei of undifferentiated and proliferating cells. We identified cytoplasmic expression of the SOX2 protein in

the immunostaining experiments. Previous studies have also reported SOX2 cytoplasmic localization [56-59].

In 2009, Baltus et al. suggested that SOX2 moves from the nucleus to the cytoplasm in response to differentiation signals [60]. In neuronal cells, cytoplasmic localization of SOX2 has also been observed [61]. Cytoplasmic localization of SOX2 in differentiated neurons seems to result from the process of differentiation-induced proteolytic degradation [60]. By contrast, nuclear SOX2 expression is lost upon differentiation [62].

In 2018, Okolicsanyi et al. indicated that SOX2 localization was distinctly cytoplasmic in MSC-induced neurosphere cultures, with a more neural progenitor-like population than the nuclear localization observed in undifferentiated human MSC and neural stem cell (NSC) cultures [63].

The same level of Nestin gene and protein expression was observed in all three culture conditions (Figures 5–6). Cell–ECM interactions, such as cell–cell interactions, played a similar role in the expression of neural progenitor cell markers. The effect of cellulosic hydrogels on the

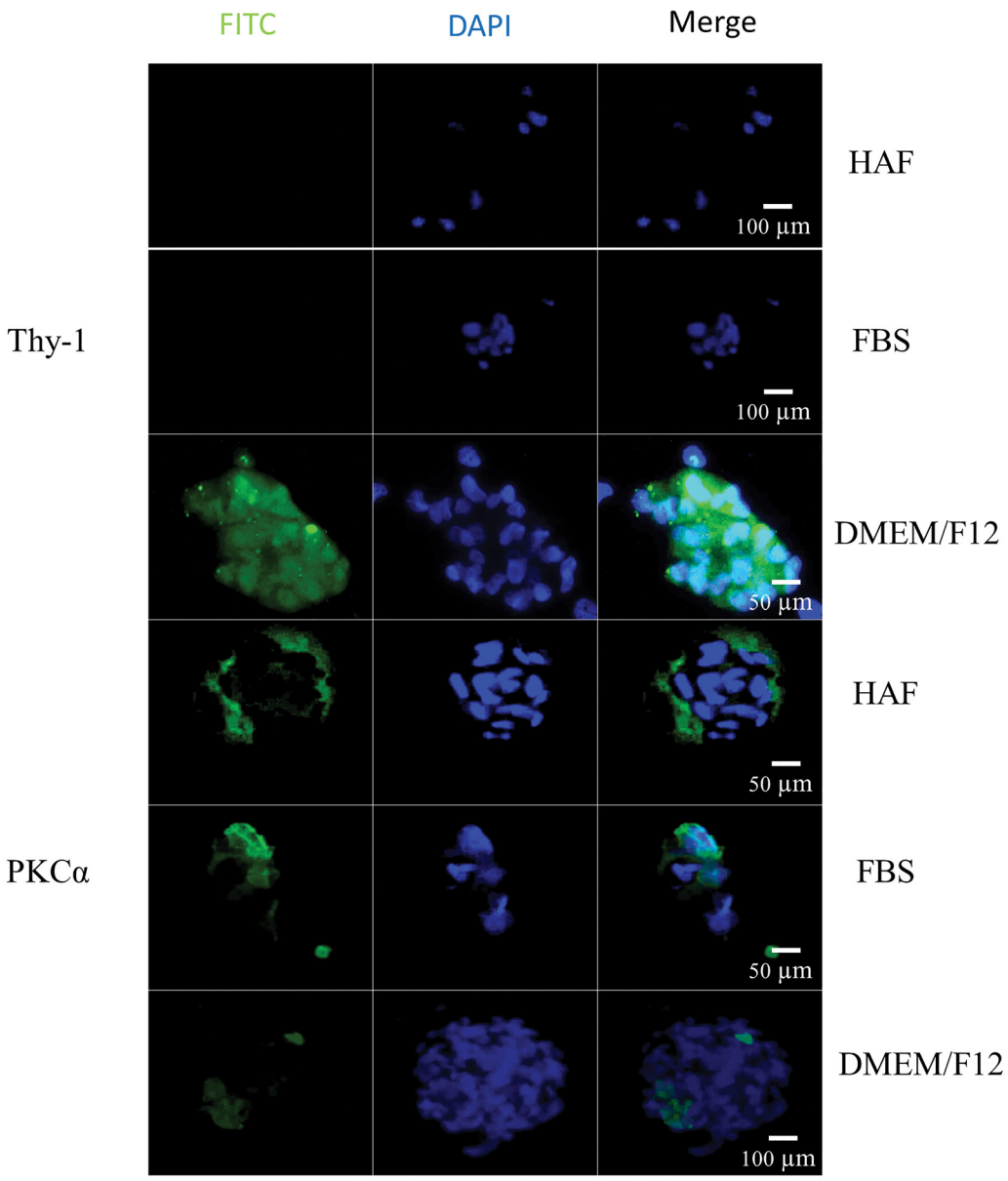

Figure 8. Immunostaining for Thy-1 and PKCα markers. Thy-1 and PKCα cytoplasmic expression in HAF, FBS, and DMEM/F12-treated hRPE cells (Passage 5) that had been cultured on A/G substrate, after 7 days. Magnification: 200X.

differentiation of MSCs into neural progenitor cells has been previously confirmed [64].

Remarkable expression of PAX6 at the mRNA transcript and protein levels was detected in all culture conditions. The highest level of PAX6 expression was observed in FBS-treated cultures (Figures 5 and 7). This suggests that cell–ECM interactions induced the appearance of neural retinal progenitor cells (NRPCs) under the corresponding conditions. NRPCs can differentiate into glial cells, various types of photoreceptors, and neurons [65]. Jasty et al. (2014) isolated stem cells from the ciliary pigment epithelium and cultivated them on nanofiber scaffolds. They demonstrated that stem cells became entrapped and formed colony-like clusters in the scaffolds. The adjoining spheroids expressed neural retinal progenitor markers, such as PAX6, and neural progenitor cell markers, such as Nestin [66].

A/G substrate induced remarkable increases in VSX-2 expression in FBS-, HAF-, and DMEM/F12-treated cultures (Figure 5 and Figure 7). Substrates played an important role in the expression of late retinal progenitor cell markers by

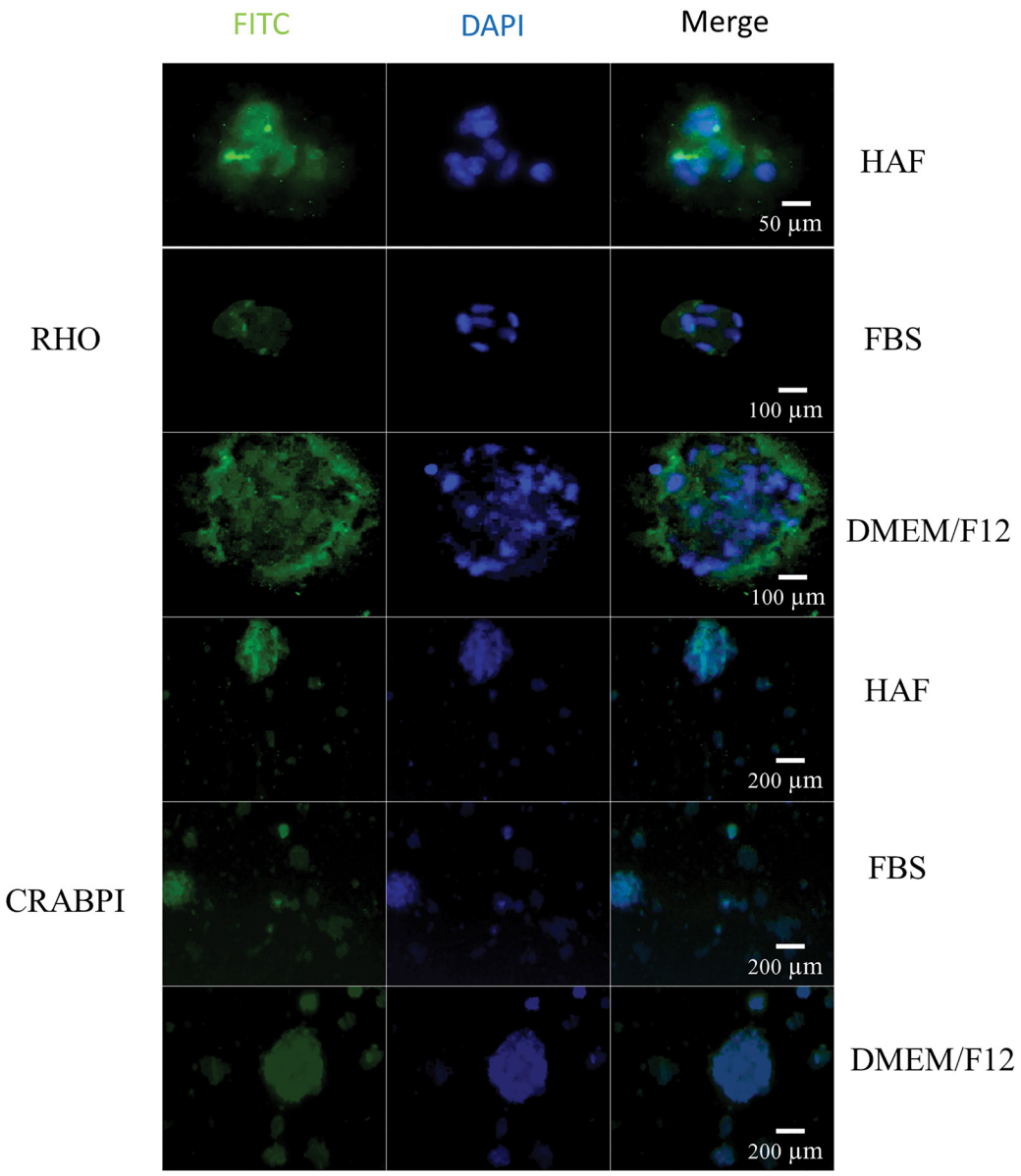

Figure 9. Immunostaining for RHO and CRABPI markers. RHO membranous expression and cytoplasmic and/or nuclear CRABPI expression in HAF, FBS, and DMEM/F12-treated hRPE cells (Passage 5) that had been cultured on A/G substrate, after 7 days. Magnification: 200X.

inducing cell–ECM interactions. Late retinal progenitor cells tended to differentiate into bipolar cells, horizontal cells, amacrine cells, rod photoreceptors, and Müller glial cells. It has also been previously shown that alginate hydrogel encapsulation improves the differentiation of human pluripotent stem cells into neural retinal cells [34].

In DMEM/F12-containing media, a few cells in large suspended spheroids exhibited Thy-1 protein expression (Figure 8), whereas mRNA expression was not detected in those cultures.

Similarly, Schlamp et al. demonstrated that ganglion 452 cell death caused a decrease in Thy1 mRNA level, with no change in the number of Thy1-expressing cells. When mouse eyes were subjected to optic nerve crush, leading to induced ganglion cell death, Thy1 mRNA level decreased within 24 h and steadily declined to nearly undetectable level by 2 weeks; however, the number of Thy1-expressing cells did not decrease for 7 days [67]. Only traces of Thy1 mRNA were detectable in N-Methyl-D-aspartate- and NMDA-injected eyes after 48 days, but Thy1 protein immunoreactivity slowly decreased over 8 days [68]. Thy-1 protein was not detected under either FBS or HAF treatment.

It is possible that the substrate, which induced cell–cell interactions, assisted in the expression of retinal ganglion cell markers. Previous studies have demonstrated the effective role of fibrin hydrogels and polybenzyl glutamate scaffolds in the differentiation of stem cells into retinal ganglion cells [69, 70].

PKCα gene expression increased fourfold in HAF-treated cultures on A/G substrates. Other treatments did not induce a remarkable increase in gene expression (Figure 5). PKCα protein expression was detected in all culture conditions (Figure 8). These findings indicate that the expression of bipolar cell markers requires an appropriate substrate to induce cell–ECM interactions in combination with growth factor supplements in culture. This finding is consistent with Tomita and colleagues' report that polylactic-coglycolic acid/poly-L-lactide acid (PLGA/PLLA) substrates increased the differentiation rate of RPCs into bipolar cells [71].

The same level of *RHO* overexpression was detected in the HAF- and FBS-treated cultures (Figure 5). Rhodopsin protein was detected in all treated cultures (Figure 9).

This likely indicates that substrate-induced cell–ECM interactions were sufficient for the expression of rod

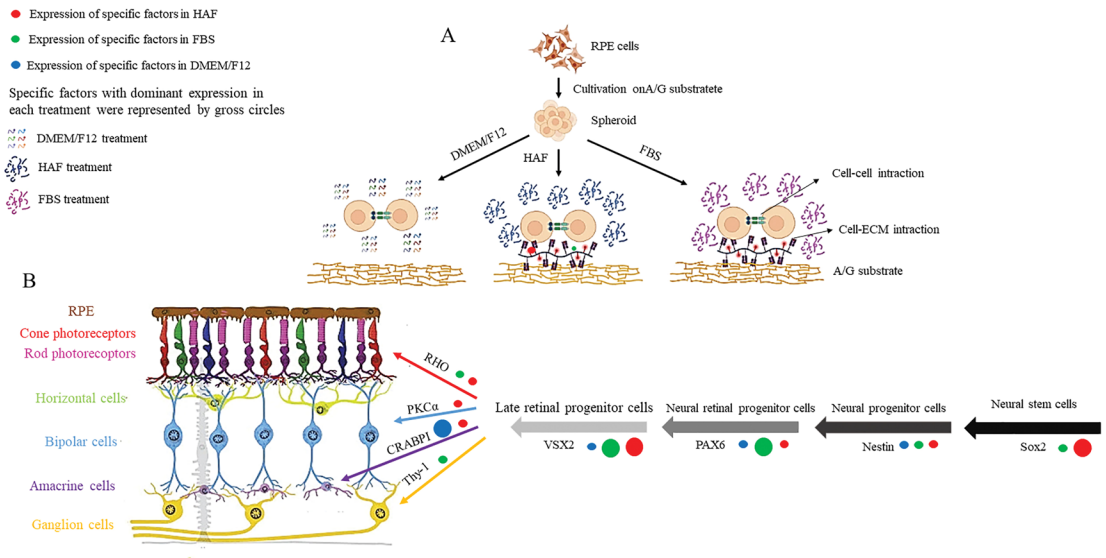

Figure 10. hRPE cells on A/G substrate. **A**: Schematic presentation of hRPE cell cultivation on A/G substrate. hRPE cells formed spheroids when they were cultured on A/G substrate. A/G substrate facilitated cell–ECM interactions when cultures were supplemented with HAF or FBS. In a DMEM/F12-treated cultures, A/G substrate directed hRPE cells to establish cell–cell interactions. **B**: Schematic presentation of stem cell differentiation into neural retinal cell lineage. The expression patterns of specific markers during differentiation are presented. Factors that are expressed in mRPE cell cultures under treatment with HAF, FBS, or DMEM/F12 are represented by red, green, and blue circles, respectively. Specific factors with dominant expression in each treatment are represented by gross circles. Figure was created with BioRender.

photoreceptor cell markers. Steedman et al. cultivated RPCs on polycaprolactone (PCL) thin film scaffolds and demonstrated cell–cell communication in clusters that appeared on the substrate and induced the differentiation of RPCs into rod photoreceptor cells [72].

A considerable increase in the protein and transcript levels of CRABPI was detected in response to different treatments on the A/G substrate (Figure 5 and Figure 9). In 2017, human fetal-derived RPCs were transplanted into the eyes of rat models with retinal degeneration. Based on the results, a phase I clinical trial was performed to confirm the safety and tolerability of transplantation in eight patients with advanced RP.

For the first time Yong Liu, et.al [73] confirmed the long-term safety and feasibility of vision repair by stem cell therapy in retinitis pigmentosa patients. Their results provided applicable information for studies related to cell-based therapies for retinitis pigmentosa and other inherited retinal degenerative disorders.

This study indicates that the proliferation and differentiation of hRPE cells on the A/G substrate relies on cell–cell interactions, cell–ECM interactions, and growth factor supplementation. In the HAF-treated culture, hRPE cells formed small, adherent spheroids similar to FBS-treated cultures. Recruitment of growth factors predominantly induced differentiation of cells toward neural stem cells and late retinal progenitor cells with high proliferative potential. The highest proliferation rate of the cultures depended on the augmentation of HAF, which is a source of various nutrient growth factors.

Under routine culture conditions of DMEM/F12 media supplemented with FBS, hRPE cells exhibited small adherent spheroids on the A/G substrate. These cell–ECM interactions predominantly induced hRPE cells to differentiate into neural retinal progenitor cells and late retinal progenitor cells, as well as terminally differentiated neural retinal cells.

Large suspended spheroids of hRPE cells were formed in DMEM/F12 culture on A/G substrate. Cell–cell interactions predominantly induced hRPE cell differentiation toward amacrine cells. The low proliferation rate in DMEM/F12-treated cultures confirmed that the culture featured terminally differentiated cells. As evidenced in this study, the A/G substrate can be recruited to generate different lineages of retinal cells in retinal regenerative studies.

Conclusions: A/G substrate improved hRPE cell survival, proliferation rate, and biologic integration with the coordination of growth factor resources. It directed the de- and transdifferentiation of hRPE cells to the neural retinal lineage through signals derived from cell (cell–cell) and substrate (cell–ECM) interactions. Our findings propose an A/G substrate for tissue engineering of the retinal nexus in the context of cell replacement therapies and future retinal regenerative research.

APPENDIX 1.

To access the data, click or select the words "Appendix 1." Negative and background controls for immunostaining. (A) and (B): Merged of DAPI and FITC photographs of hRPE cells that had been recruited in immunostaining assay without primary rabbit anti-human antibody and without applying primary and secondary antibodies, respectively. Magnification: 200X.

APPENDIX 2.

To access the data, click or select the words "Appendix 2." Negative and background controls for immunostaining assays. (A), (B), (C) and (D): Merged of DAPI and FITC photographs of hRPE cells that had been recruited in immunostaining assay without primary rabbit anti-human, mouse anti-human and goat anti-human antibodies and without applying primary and secondary antibodies, respectively. Magnification: 200X

ACKNOWLEDGMENTS

This work was supported by Iran National Science Foundation through grant number of 97009298, National Institute for Medical Research Development (NIMAD) through grant number of 964465 and National Institute of Genetic Engineering and Biotechnology (NIGEB), Tehran, Iran through grant number of 715. We wish to acknowledge Meisam Lesani and Maliheh Davari for their contribution in completing this work. The manuscript was presented in the 9th annual meeting of the Iranian research association for vision and ophthalmology. **Authorship:** H.SHN. performed the experiments, participated in the design of the experiments and data analysis, and wrote the manuscript. Z-S.S. participated in the design of the experiments and data analysis, edited the manuscript, provided the budget and supervised the study. SH.S. performed the experiments. H.A. participated in the preparation and editing of the manuscript. E.RP. participated in the design of the experiments. M.H. participated in HAF preparation. **Funding:** This work was supported by Iran National Science Foundation through grant number of 97,009,298, National Institute for Medical Research Development (NIMAD) through grant number of 964,465 and National Institute of Genetic Engineering and Biotechnology (NIGEB), Tehran, Iran through grant number of 715. **Data Availability Statement:** The data that support the findings of

this study are available from the corresponding author upon reasonable request.

REFERENCES

1. Binder S, Stanzel B, Krebs I, Glittenberg C. Transplantation of the RPE in AMD. Prog Retin Eye Res 2007; 26:516-54. [PMID: 17532250].
2. Schwartz SD, Regillo CD, Lam BL, Eliott D, Rosenfeld PJ, Gregori NZ, Hubschman J-P, Davis JL, Heilwell G, Spirn M, Maguire J, Gay R, Bateman J, Ostrick RM, Morris D, Vincent M, Anglade E, Del Priore LV, Lanza R. Human embryonic stem cell-derived retinal pigment epithelium in patients with age-related macular degeneration and Stargardt's macular dystrophy: follow-up of two open-label phase 1/2 studies. Lancet 2015; 385:509-516[PMID: 25458728].
3. Falkner-Radler CI, Krebs I, Glittenberg C, Považay B, Drexler W, Graf A, Binder S. Human retinal pigment epithelium (RPE) transplantation: outcome after autologous RPE-choroid sheet and RPE cell-suspension in a randomised clinical study. Br J Ophthalmol 2011; 95:370-5[PMID: 20610478].
4. Qiu G, Seiler MJ, Mui C, Arai S, Aramant RB. Juan Jr Ed, Sadda S. Photoreceptor differentiation and integration of retinal progenitor cells transplanted into transgenic rats. Exp Eye Res 2005; 80:515-25. [PMID: 15781279].
5. Falkner-Radler CI, Krebs I, Glittenberg C, Považay B, Drexler W, Graf A, Binder S. Human retinal pigment epithelium (RPE) transplantation: outcome after autologous RPE-choroid sheet and RPE cell-suspension in a randomised clinical study. Br J Ophthalmol 2011; 95:370-[PMID: 20610478].
6. Tang Z, Zhang Y, Wang Y, Zhang D, Shen B, Luo M, Gu P. Progress of stem/progenitor cell-based therapy for retinal degeneration. J Transl Med 2017; 15:99-[PMID: 28486987].
7. da Cruz L, Chen F, Ahmado A, Greenwood J, Coffey P. RPE transplantation and its role in retinal disease. Prog Retin Eye Res 2007; 26:598-635. [PMID: 17920328].
8. Casaroli-Marano RP, Zarbin MA. Cell-Based Therapy for Retinal Degenerative Disease: Karger Medical and Scientific Publishers; 2014.
9. Sharma R, Bose D, Maminishkis A, Bharti K. Retinal Pigment Epithelium Replacement Therapy for Age-Related Macular Degeneration: Are We There Yet? Annu Rev Pharmacol Toxicol 2020; 60:553-72. [PMID: 31914900].
10. Yao J, Tao SL, Young MJ. Synthetic Polymer Scaffolds for Stem Cell Transplantation in Retinal Tissue Engineering. Polymers (Basel) 2011; 3:899-914. .
11. Magatti M, Vertua E, Cargnoni A, Silini A, Parolini O. The Immunomodulatory Properties of Amniotic Cells: The Two Sides of the Coin. Cell Transplant 2018; 27:31-44. [PMID: 29562786].
12. Sanie-Jahromi F, Ahmadieh H, Soheili Z-S, Davari M, Ghaderi S, Kanavi MR, Samiei S, Deezagi A, Pakravesh J, Bagheri A. Enhanced generation of retinal progenitor cells from human retinal pigment epithelial cells induced by amniotic fluid. BMC Res Notes 2012; 5:182-[PMID: 22490806].
13. Ghaderi S, Soheili Z, Ahmadieh H, Davari M, Jahromi F, Samie S, Rezaie-Kanavi M, Pakravesh J, Deezagi A. Human Amniotic Fluid Promotes Retinal Pigmented Epithelial Cells'Trans-Differentiation into Rod Photoreceptors and Retinal Ganglion Cells. Stem Cells Dev 2011; 20:1615-25. [PMID: 21142973].
14. Davari M, Soheili Z-S, Ahmadieh H, Sanie-Jahromi F, Ghaderi S, Kanavi MR, Samiei S, Akrami H, Haghighi M, Javidi-Azad F. Amniotic fluid promotes the appearance of neural retinal progenitors and neurons in human RPE cell cultures. Mol Vis 2013; 19:2330-[PMID: 24265548].
15. Rahmani Del Bakhshayesh A, Annabi N, Khalilov R, Akbarzadeh A, Samiei M, Alizadeh E, Alizadeh-Ghodsi M, Davaran S, Montaseri AJ. Recent advances on biomedical applications of scaffolds in wound healing and dermal tissue engineering. Artif Cells Nanomed Biotechnol 2018; 46:691-705. [PMID: 28697631].
16. Wu Z, Su X, Xu Y, Kong B, Sun W, Mi S. Bioprinting three-dimensional cell-laden tissue constructs with controllable degradation. Sci Rep 2016; 6:24474-[PMID: 27091175].
17. Chan BP, Leong KW. Scaffolding in tissue engineering: general approaches and tissue-specific considerations. Eur Spine J 2008; 17:Suppl 4467-79. [PMID: 19005702].
18. Rose JB, Pacelli S, Haj AJE, Dua HS, Hopkinson A, White LJ, Rose FR. Gelatin-Based Materials in Ocular Tissue Engineering. Materials (Basel) 2014; 7:3106-35. [PMID: 28788609].
19. Jeong SM, Kim EY, Hwang JH, Lee GY, Cho SJ, Bae JY, Song JE, Yoon KH, Joo C-K, Lee D. A Study on Proliferation and Behavior of Retinal Pigment Epithelial Cells on Purified Alginate Films. Int J Stem Cells 2011; 4:105-[PMID: 24298342].
20. Cascone S. Lamberti GJIjop. Hydrogel-based commercial products for biomedical applications RE:view 2020; 573:118803-[PMID: 31682963].
21. Rahmani Del Bakhshayesh A, Annabi N, Khalilov R, Akbarzadeh A, Samiei M, Alizadeh E, Alizadeh-Ghodsi M, Davaran S, Montaseri A. Recent advances on biomedical applications of scaffolds in wound healing and dermal tissue engineering. Artif Cells Nanomed Biotechnol 2018; 46:691-705. [PMID: 28697631].
22. Cascone S, Lamberti G. Hydrogel-based commercial products for biomedical applications: A review. Int J Pharm 2020; 573:118803-[PMID: 31682963].
23. Li J, Wu C, Chu PK, Gelinsky M. 3D printing of hydrogels: Rational design strategies and emerging biomedical applications. Mater Sci Eng Rep 2020; 140:100543-.
24. Aswathy SH, Narendrakumar U, Manjubala I. Commercial hydrogels for biomedical applications. Heliyon 2020; 6:e03719-[PMID: 32280802].
25. Nawaz S, Khan S, Farooq U, Haider MS, Ranjha NM, Rasul A, Nawaz A, Arshad N, Hameed R. Polymers. Biocompatible

hydrogels for the controlled delivery of anti-hypertensive agent: development, characterization and in vitro evaluation. Des Monomers Polym 2018; 21:18-32. .

26. Rahmani Del Bakhshayesh A, Annabi N, Khalilov R, Akbarzadeh A, Samiei M, Alizadeh E, Alizadeh-Ghodsi M, Davaran S, Montaseri A. Recent advances on biomedical applications of scaffolds in wound healing and dermal tissue engineering. Artif Cells Nanomed Biotechnol 2018; 46:691-705. [PMID: 28697631].

27. Łabowska MB, Cierluk K, Jankowska AM, Kulbacka J, Detyna J, Michalak I. A Review on the Adaption of Alginate-Gelatin Hydrogels for 3D Cultures and Bioprinting. Materials (Basel, Switzerland). 2021;14.

28. Syed SS, Kulkarni D, Todkar R, Bagul RS, Parekh K, Bhujbal N. A novel method of coating orthodontic archwires with nanoparticles. J Int Oral Health 2015; 7:30-3. [PMID: 26028899].

29. Naahidi S, Jafari M, Logan M, Wang Y, Yuan Y, Bae H, Dixon B, Chen P. Biocompatibility of hydrogel-based scaffolds for tissue engineering applications. Biotechnol Adv 2017; 35:530-44. [PMID: 28558979].

30. Andersen T, Auk-Emblem P, Dornish M. 3D Cell Culture in Alginate Hydrogels. Microarrays (Basel) 2015; 4:133-61. [PMID: 27600217].

31. Montalbano G, Toumpaniari S, Popov A, Duan P, Chen J, Dalgarno K, Scott WE, Ferreira AM. Synthesis of bioinspired collagen/alginate/fibrin based hydrogels for soft tissue engineering. Mater Sci Eng C 2018; 91:236-46. [PMID: 30033251].

32. Shams Najafabadi H, Soheili Z-S, Mohammad Ganji S. Studying the Morphology and Growth of Human Retinal Pigment Epithelial Cells on a Thin Layer of Alginate and Alginate/Gelatin as a Culture Substrate. Modares Journal of Medical Sciences: Pathobiology. 2013; 16:81-93. .

33. Tada H, Shiho O, Kuroshima K-i, Koyama M, Tsukamoto K. An improved colorimetric assay for interleukin 2. J Immunol Methods 1986; 93:157-65. [PMID: 3490518].

34. Hunt NC, Hallam D, Karimi A, Mellough CB, Chen J, Steel DHW, Lako M. 3D culture of human pluripotent stem cells in RGD-alginate hydrogel improves retinal tissue development. Acta Biomater 2017; 49:329-43. [PMID: 27826002].

35. Stanzel BV, Liu Z, Somboonthanakij S, Wongsawad W, Brinken R, Eter N, Corneo B, Holz FG, Temple S, Stern JH, Blenkinsop TA. Human RPE stem cells grown into polarized RPE monolayers on a polyester matrix are maintained after grafting into rabbit subretinal space. Stem Cell Reports 2014; 2:64-77. [PMID: 24511471].

36. Liao J-L, Yu J, Huang K, Hu J, Diemer T, Ma Z, Dvash T, Yang X-J, Travis GH, Williams DS, Bok D, Fan G. Molecular signature of primary retinal pigment epithelium and stem-cell-derived RPE cells. Hum Mol Genet 2010; 19:4229-38. [PMID: 20709808].

37. Chen C-Y, Ke C-J, Yen K-C, Hsieh H-C, Sun J-S, Lin F-H. 3D Porous Calcium-Alginate Scaffolds Cell Culture System Improved Human Osteoblast Cell Clusters for Cell Therapy. Theranostics 2015; 5:643-55. [PMID: 25825603].

38. Bae Y-J, Kwon Y-R, Kim HJ, Lee S, Kim Y-J. Enhanced differentiation of mesenchymal stromal cells by three-dimensional culture and azacitidine. Blood Res 2017; 52:18-24. [PMID: 28401097].

39. Ferro F, Baheney CS, Spelat R. Three-Dimensional (3D) Cell Culture Conditions, Present and Future Improvements. Razavi International Journal of Medicine. 2014; 2:2-.

40. Bozza A, Coates EE, Incitti T, Ferlin KM, Messina A, Menna E, Bozzi Y, Fisher JP, Casarosa S. Neural differentiation of pluripotent cells in 3D alginate-based cultures. Biomaterials 2014; 35:4636-45. [PMID: 24631250].

41. Shaobo ZHU, Tao Z, Chen SUN, Aixi YU, Baiwen QI, Hao C. Bone marrow mesenchymal stem cells combined with calcium alginate gel modified by hTGF-β1 for the construction of tissue-engineered cartilage in three-dimensional conditions. Exp Ther Med 2013; 5:[PMID: 23251248].

42. Torisawa YS, Takagi A, Nashimoto Y, Yasukawa T, Shiku H, Matsue T. A multicellular spheroid array to realize spheroid formation, culture, and viability assay on a chip. Biomaterials 2007; 28:559-66. [PMID: 16989897].

43. Steadman K, Stein WD, Litman T, Yang SX, Abu-Asab M, Dutcher SK, Bates S. PolyHEMA spheroids are an inadequate model for the drug resistance of the intractable solid tumors. Cell Cycle 2008; 7:818-29. [PMID: 18239467].

44. Dhoot NO, Tobias CA, Fischer I, Wheatley MA. Peptide-modified alginate surfaces as a growth permissive substrate for neurite outgrowth. J Biomed Mater Res A 2004; 71:191-200. [PMID: 15376189].

45. Wang L, Shelton R, Cooper P, Lawson M, Triffitt J, Barralet J. Evaluation of sodium alginate for bone marrow cell tissue engineering. Biomaterials 2003; 24:3475-81. [PMID: 12809776].

46. Gnanaprakasam Thankam F, Muthu J, Sankar V, Kozhiparambil Gopal R. Growth and survival of cells in biosynthetic poly vinyl alcohol–alginate IPN hydrogels for cardiac applications. Colloids Surf B Biointerfaces 2013; 107:137-45. [PMID: 23475061].

47. Najafabadi HS, Soheili Z-S, Ganji SM. Behavior of a Spontaneously Arising Human Retinal Pigment Epithelial Cell Line Cultivated on Thin Alginate Film. J Ophthalmic Vis Res 2015; 10:286-94. [PMID: 26730315].

48. Heidari R, Soheili Z-S, Samiei S, Ahmadieh H, Davari M, Nazemroaya F, Bagheri A, Deezagi A. Alginate as a Cell Culture Substrate for Growth and Differentiation of Human Retinal Pigment Epithelial Cells. Appl Biochem Biotechnol 2015; 175:2399-412. [PMID: 25502925].

49. Chrissouli S, Pratsinis H, Velissariou V, Anastasiou A, Kletsas D. Human amniotic fluid stimulates the proliferation of human fetal and adult skin fibroblasts: The roles of bFGF and PDGF and of the ERK and Akt signaling pathways. Wound Repair Regen 2010; 18:643-54. [PMID: 20946138].

50. Kimura Y, Madhavan M, Call MK, Santiago W, Tsonis PA, Lambris JD, Del Rio-Tsonis K. Expression of complement 3 and complement 5 in newt limb and lens regeneration. J Immunol 2003; 170:2331-9. [PMID: 12594255].

51. Reca R, Mastellos D, Majka M, Marquez L, Ratajczak J, Franchini S, Glodek A, Honczarenko M, Lynn A Spruce AJ-W, John D. Lambris, Mariusz Z Ratajczak. Functional receptor for C3a anaphylatoxin is expressed by normal hematopoietic stem/progenitor cells, and C3a enhances their homing-related responses to SDF-1. Blood 2003; 101:3784-93. [PMID: 12511407].

52. Cooper GM. Cell Proliferation in Development and Differentiation. The Cell: A Molecular Approach. 2nd edition. 2000.

53. Das AV, Edakkot S, Thoreson WB, James J, Bhattacharya S, Ahmad I. Membrane properties of retinal stem cells/progenitors. Prog Retin Eye Res 2005; 24:663-81. [PMID: 15939659].

54. Schmitt S, Aftab U, Jiang C, Redenti S, Klassen H, Miljan E, Sinden J, Young M. Molecular characterization of human retinal progenitor cells. Invest Ophthalmol Vis Sci 2009; 50:5901-8. [PMID: 19553622].

55. Gao S, Zhao P, Lin C, Sun Y, Wang Y, Zhou Z, Yang D, Wang X, Xu H, Zhou F, Cao L, Zhou W, Ning K, Chen X, Xu J. Differentiation of Human Adipose-Derived Stem Cells into Neuron-Like Cells Which Are Compatible with Photocurable Three-Dimensional Scaffolds. Tissue Eng Part A 2014; 20:1271-84. [PMID: 24251600].

56. Pan H, Schultz RM. Sox2 modulates reprogramming of gene expression in two-cell mouse embryos. Biol Reprod 2011; 85:409-16. [PMID: 21543769].

57. Avilion AA, Nicolis SK, Pevny LH, Perez L, Vivian N, Lovell-Badge R. Multipotent cell lineages in early mouse development depend on SOX2 function. Genes Dev 2003; 17:126-40. [PMID: 12514105].

58. Schaefer T, Lengerke C. SOX2 protein biochemistry in stemness, reprogramming, and cancer: the PI3K/AKT/SOX2 axis and beyond. Oncogene 2020; s39:1-15. [PMID: 31477842].

59. Volpato T, Tesser RB, Nunes M, Stumpp T. Dynamics of Sox2 expression during rat germ cell development and its relationship with emergence of spermatogonia. bioRxiv 2019; x:558015-.

60. Baltus GA, Kowalski MP, Zhai H, Tutter AV, Quinn D, Wall D, Kadam S. Acetylation of Sox2 Induces its Nuclear Export in Embryonic Stem Cells. Stem Cells 2009; 27:2175-84. [PMID: 19591226].

61. Annovazzi L, Mellai M, Caldera V, Valente G, Schiffer D. SOX2 expression and amplification in gliomas and glioma cell lines. Cancer Genomics Proteomics 2011; 8:139-47. [PMID: 21518820].

62. Uwanogho D, Rex M, Cartwright EJ, Pearl G, Healy C, Scotting PJ, Sharpe PT. Embryonic expression of the chicken Sox2, Sox3 and Sox11 genes suggests an interactive role in neuronal development. Mech Dev 1995; 49:23-36. [PMID: 7748786].

63. Okolicsanyi RK, Oikari LE, Yu C, Griffiths LR, Haupt LM. Heparan Sulfate Proteoglycans as Drivers of Neural Progenitors Derived From Human Mesenchymal Stem Cells. Front Mol Neurosci 2018; 11: 134-[PMID: 29740281].

64. Gu H, Yue Z, Leong WS, Nugraha B, Tan LP. Control of in vitro neural differentiation of mesenchymal stem cells in 3D macroporous, cellulosic hydrogels. Regen Med 2010; 5:245-53. [PMID: 20210584].

65. Phillips MJ, Jiang P, Howden S, Barney P, Min J, York NW, Chu L-F, Capowski EE, Cash A, Jain S, Barlow K, Tabassum T, Stewart R, Pattnaik BR, Thomson JA, Gamm DM. A Novel Approach to Single Cell RNA-Sequence Analysis Facilitates In Silico Gene Reporting of Human Pluripotent Stem Cell-Derived Retinal Cell Types. Stem Cells 2018; 36:313-24. [PMID: 29230913].

66. Jasty S, Suriyanarayanan S, Krishnakumar S. Influence of self-assembling peptide nanofibre scaffolds on retinal differentiation potential of stem/progenitor cells derived from ciliary pigment epithelial cells. Tissue Eng Regen Med 2014; [PMID: 25066608].

67. Schlamp CL, Johnson EC, Li Y, Morrison JC, Nickells RW. Changes in Thy1 gene expression associated with damaged retinal ganglion cells. Mol Vis 2001; 7:192-201. [PMID: 11509915].

68. Nash MS, Osborne NN. Assessment of Thy-1 mRNA levels as an index of retinal ganglion cell damage. Invest Ophthalmol Vis Sci 1999; 40:1293-8. [PMID: 10235569].

69. Roozafzoon R, Lashay A, Vasei M, Ai J, Khoshzaban A, Keshel SH, Barabadi Z, Bahrami H. Dental pulp stem cells differentiation into retinal ganglion-like cells in a three dimensional network. Biochem Biophys Res Commun 2015; 457:154-60. [PMID: 25543058].

70. Chen T-C, She P-Y, Chen DF, Lu J-H, Yang C-H, Huang D-S, Chen P-Y, Lu C-Y, Cho K-S, Chen H-F, Su W-F. Polybenzyl Glutamate Biocompatible Scaffold Promotes the Efficiency of Retinal Differentiation toward Retinal Ganglion Cell Lineage from Human-Induced Pluripotent Stem Cells. Int J Mol Sci 2019; 20:178-[PMID: 30621308].

71. Tomita M, Lavik E, Klassen H, Zahir T, Langer R, Young MJ. Biodegradable Polymer Composite Grafts Promote the Survival and Differentiation of Retinal Progenitor Cells. Stem Cells 2005; 23:1579-88. [PMID: 16293582].

72. Steedman MR, Tao S, Klassen H, Desai T. Enhanced differentiation of retinal progenitor cells using microfabricated topographical cues. Biomed Microdevices 2010; 12:363-9. [PMID: 20077017].

73. Liu Y, Chen SJ, Li SY, Qu LH, Meng XH, Wang Y, Xu HW, Liang ZQ, Yin ZQ. Long-term safety of human retinal progenitor cell transplantation in retinitis pigmentosa patients. Stem Cell Res Ther 2017; 8:209-[PMID: 28962643].

Articles are provided courtesy of Emory University and the Zhongshan Ophthalmic Center, Sun Yat-sen University, P.R. China. The print version of this article was created on 12 December 2022. This reflects all typographical corrections and errata to the article through that date. Details of any changes may be found in the online version of the article.